journal

J. Am. Ceram. Soc., 85 [3] 675–82 (2002)

Coarsening of Faceted Crystals

Gregory S. Rohrer,* C. Lane Rohrer, and William W. Mullins†

Department of Materials Science and Engineering, Carnegie Mellon University, Pittsburgh, Pennsylvania 15213-3890

The influence of the nucleation energy barrier on the capillary-driven coarsening of faceted crystals that exchange material by diffusion is quantified. Our calculations are based on the assumption that the transport of material between particles must happen in series with the nucleation of partial layers on flat facets. Using a numerical model based on this idea, we simulate the time evolution of distributions of crystals that are made up of perfect faceted crystals (without step-producing defects), crystals containing step-producing defects, and mixtures of the two types. We find that the coarsening of a distribution containing only perfect faceted crystals is arrested at a size where the nucleation energy barrier becomes prohibitive. This critical size ranges from a few nanometers to several hundred nanometers, depending on material parameters and experimental conditions. When a small fraction of the crystals have step-producing defects (for these crystals the nucleation energy barrier vanishes), they can grow to large sizes at the expense of the perfect crystals and a bimodal grain size distribution is created. Based on these results, we hypothesize that when abnormal coarsening is observed in nature, it results from the presence of a small number of crystals with step-producing defects.

I. Introduction

THE conventionally accepted theory for coarsening established by Lifshitz, Slyozov,[1] and Wagner[2] (LSW) assumes that crystals grow (or shrink) by the addition (or removal) of atoms that are transported to (or away from) the crystal by capillary-driven diffusion. The assumption that the rates of growth and dissolution are limited by the rate of atomic diffusion implies that the surface attachment process is relatively rapid. This assumption seems to be appropriate for crystals with rough surfaces or crystals where the surfaces have step-producing defects. However, there is a well-known nucleation (free) energy barrier (NEB) for the addition or removal of atoms from an ideal flat facet.[3] The purpose of the present paper is to describe the influence of the NEB on the capillary-driven coarsening of faceted crystals.

In our coarsening model, we adopt the mean field approach in which exchanges of material between particles are represented by exchanges between a particle and a reservoir at the chemical potential μ_∞ of the substance (with $\mu = 0$ for the bulk material with a flat surface), where the value of μ_∞ is chosen to conserve material. Our numerical treatment assumes that the particles are fully faceted, but some discussion is given of the partially faceted case in which the equilibrium crystal shape (ECS) of the particles contains smoothly curved regions of surface as well as facets. Our assumption of a fully faceted form implies that for a crystal to change size while retaining its shape, new layers of atoms must be added to or subtracted from the facets. For this to happen, the crystal must pass through a relatively higher energy state where there is a partial layer (or nucleus) on a facet. Because of this higher energy state, there is a NEB proportional to the crystal size that must be overcome by a thermal fluctuation in order for coarsening to proceed. In general, there are NEBs for both particle growth and particle dissolution; these are equal at equilibrium.[4,5] It is the presence of this thermally activated process or fluctuation that distinguishes the coarsening of faceted crystals from that of nonfaceted or rough crystals. We, therefore, construct our model with the assumption that two processes must occur in series: diffusion through the medium that supplies and removes material from the crystals and the nucleation events necessary for the advance or retreat of a facet.

In our simulations, we separately consider perfect crystals (without step-producing defects), crystals containing step-producing defects, and mixtures of the two. We show that for crystals without step-producing defects, coarsening comes to a stop, typically for particle sizes above a few nanometers or a few tens of nanometers, depending on physical parameters selected for the calculation. In this case, coarsening ceases because of the prohibitive size of the NEBs for facet motion. For crystals that contain step-producing defects, there is no NEB and our model simply reproduces the results of LSW theory. When the starting population consists of a mixture of defective and ideal crystals, a bimodal population can develop where those crystals that do not have an NEB act as sinks for material and grow much larger than the ideal crystals. In this case, abnormal coarsening occurs.

Based on our results, we hypothesize that when exaggerated coarsening is observed in nature, it is because some of the crystals contain step-producing defects such as screw dislocations. In other words, the few giant particles observed in exaggerated coarsening contain defects (i.e., screw dislocations) that produce persistent steps on the facet surfaces so that nucleation is not required for the advance or retreat of a facet. In the next section, we describe the physical model used in our simulations. In Section III, the numerical methods used in the simulations are described. The results of the calculations are presented in Section IV. In Section V, the results are discussed and compared to previous theoretical and experimental reports. Section VI offers a summary.

II. Description of the Model

(1) Qualitative Description

To develop an approximate treatment of diffusion through the medium and layer nucleation on a facet as processes operating in series, we imagine a spherical shell of radius R' superimposed on each particle. On the surface of this shell, we impose a uniform chemical potential, μ_s, intermediate between the chemical potential far from the particle, μ_∞, and the chemical potential in equilibrium with the particle, μ_e. The value of μ_s is then chosen so that the steady-state fluxes at the shell due to diffusion match those due to nucleation. For simplicity, we suppose that all particle

L.-Q. Chen—contributing editor

Manuscript No. 187533. Received August 13, 2001; approved January 4, 2002.
This work was supported primarily by the National Aeronautics and Space Administration under Grant No. 8-1674 and partially by the MRSEC program of the National Science Foundation under Award No. DMR-0079996.
*Member, American Ceramic Society.
†Posthumous contribution.

facets are energetically equivalent and lie at the same distance R from the origin of the crystal so that

$$\mu_e = 2\sigma/R \tag{1}$$

where σ is the free energy of any one of the facets. For example, the chemical potential of a cube of side L is $\mu_e = 4\sigma/L$, since $R = L/2$. The exact position of the imaginary shell's surface is not critical, but it should be as close as possible to the surface of the cube. We make the approximation that $R = R'$ and use this as a measure of the size of the crystal, as illustrated schematically in Fig. 1(a).

If $\mu_e = \mu_s = \mu_\infty$, the particle is in equilibrium with the medium. Denoting the equilibrium value of R by R^* and using Eq. (1), we have

$$R^* = 2\sigma/\mu_\infty \tag{2}$$

Growth of a particle will occur if $\mu_e < \mu_s < \mu_\infty$, or from Eqs. (1) and (2), if $R > R^*$, whereas dissolution will occur if $\mu_e > \mu_s > \mu_\infty$, or if $R < R^*$.

We introduce two variables used in the calculations which relate to the three chemical potentials, $\rho = R/R^*$ and $\xi = \mu_s/\mu_\infty$. From the above, equilibrium corresponds to $\rho = \xi = 1$, growth to the values $\rho > 1$ and $\xi < 1$, and steady-state dissolution to the values $\rho < 1$ and $\xi > 1$. Further, from the definitions, $\rho\xi = \mu_s/\mu_e$ so that growth corresponds to $\rho\xi > 1$ and dissolution to $\rho\xi < 1$.

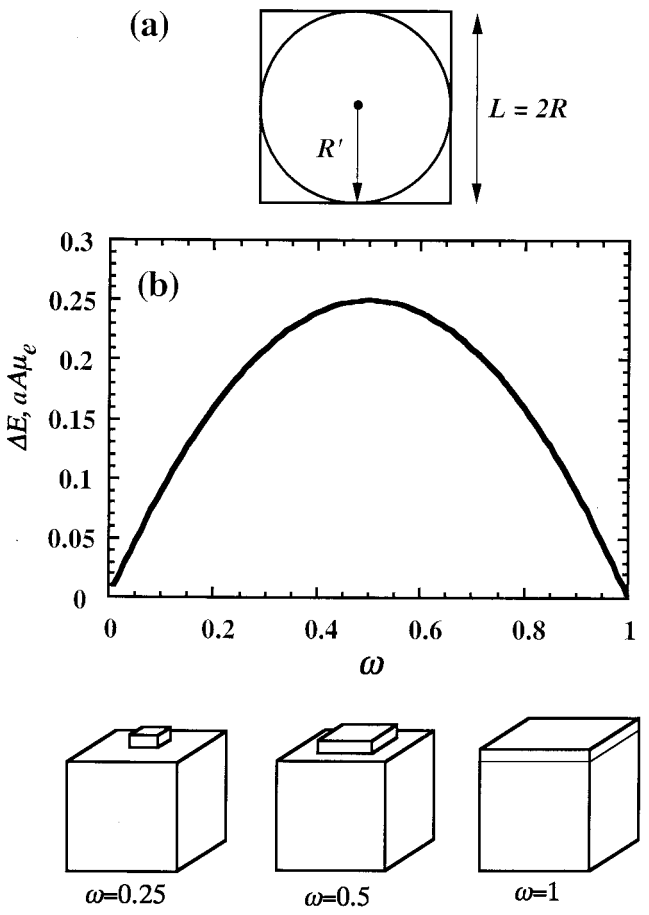

Fig. 1. (a) Schematic illustrating the relation between a cross section of the crystal and the imaginary sphere whose surface is assigned the chemical potential, μ_s. (b) Schematic illustration of the energy barrier as a function of ω (for a cubic crystal with the size R^*) and the partial layer that nucleates and grows on the surface. Note that when $\omega = 1$, the total amount of added surface energy ($4aL\sigma$) exactly balances the energy change of the material taken from the reservoir at $\mu_s(L^2a\mu_s = 4aL\sigma$ when $\mu_s = \mu_e = 2\sigma/R$).

We shall proceed as follows: First we find an expression for the growth rate of the particle due to diffusion as

$$\dot{R}_{\text{diff}} = f(R^*,\rho,\xi) \tag{3}$$

where f is a well-known function from applied diffusion theory to be specified below. Next we develop the growth rate due to nucleation as

$$\dot{R}_{\text{nucl}} = g(R^*,\rho,\xi) \tag{4}$$

where g is to be determined. Then, for the processes to operate in series, we require

$$\dot{R}_{\text{diff}} = \dot{R}_{\text{nucl}} = \dot{R} \tag{5}$$

Equation (5) is solved for $\xi(\rho, R^*)$. Substitution of this expression back into either Eq. (3) or Eq. (4) gives the growth rate as a function of ρ and R^*,

$$\dot{R} = f(R^*,\rho) \tag{6}$$

To estimate whether diffusion or nucleation is rate limiting, consider, for the moment, a growing particle. For such a particle, the fraction $f_d = (\mu_\infty - \mu_s)/(\mu_\infty - \mu_e)$ of the total chemical potential drop is devoted to driving diffusion and the fraction $f_n = (\mu_s - \mu_e)/(\mu_\infty - \mu_e)$ is devoted to driving nucleation, where both f's are positive and $f_d + f_n = 1$. Exactly the same result applies for dissolution. Clearly, the major part of the energy expenditure will be used to drive diffusion if $f_n \ll 1$. In terms of ρ and ξ, we find this condition to be

$$f_n = \frac{\rho\xi - 1}{\rho - 1} \ll 1 \tag{7}$$

As expected, the expression becomes indeterminate at equilibrium.

(2) Diffusion Process

For the diffusion calculation, we have

$$\dot{R}_{\text{diff}} = D_m\nabla(c)_R = \left(\frac{cD_m\Omega}{kT}\right)\nabla(\mu)_R \tag{8}$$

where c is the concentration of solute in the medium, D_m is the diffusion coefficient of the solute in the medium, Ω is the atomic volume, k is Boltzmann's constant, and T is the absolute temperature. Assuming the solute is dilute and that the system exhibits Henrian behavior, we have used $\Omega\nabla\mu/kT = \nabla c/c$, in which μ is expressed as energy per unit volume. The subscripts indicate that the gradients are to be evaluated at the surface of the enclosing sphere so that

$$\nabla(\mu)_R = \frac{\mu_\infty - \mu_s}{R} = \frac{\mu_\infty(1-\xi)}{R} \tag{9}$$

Therefore, using Eq. (9) and the definitions for ρ and ξ we find

$$\dot{R}_{\text{diff}} = \frac{A_{\text{diff}}(1-\xi)}{\rho(R^*)^2} \tag{10}$$

where $A_{\text{diff}} = 2\sigma cD_m\Omega/kT$. Equation (10) confirms that growth or dissolution occurs respectively as ξ is less than or greater than unity. Using $\sigma = 1$ J/m^2, $c = 10^{-2}$, $D_m = 10^{-9}$ m^2/s, $\Omega = 10^{-30}$ m^3, and $kT = 10^{-20}$ J, then, to an order of magnitude, $A_{\text{diff}} = 10^{-21}$ m^3/s.

(3) Nucleation Process

The nucleation rate, I (nuclei per unit area per unit time), on a facet is taken to be

$$I = C\{e^{-E^+/kT} - e^{-E^-/kT}\} \tag{11}$$

where E^+ is the nucleation barrier for the addition of a layer and E^- is that for the removal of a layer. It is clear that (on the average) growth due to nucleation will occur if $E^+ < E^-$ and dissolution

due to nucleation will occur if $E^+ > E^-$; the condition $E^+ = E^-$ yields $I = 0$ and represents equilibrium. We defer the estimate of C and first consider the calculation of E^+ and E^-.

We assume provisionally that particles of all sizes have the ECS; this assumption will be modified later, but will not affect the essential results. The free energy required to form a nucleus of the same shape as the facet, but smaller by a linear scale factor ω, where $0 \le \omega \le 1$, from material drawn from the reservoir at chemical potential μ_s is

$$\Delta E(\omega) = \omega a \oint \sigma_p \, dl - \omega^2 aA\mu_s \tag{12}$$

where σ_p is the orientation-dependent perimeter energy of the nucleus, assumed to be the same as the step energy on the facet.[5] The line integral is conducted around the nucleus edge when the latter coincides with the facet edge ($\omega = 1$), a is the height of the nucleus, and A is the facet area. Since $\omega = 1$ at equilibrium ($\mu_s = \mu_e$), $\Delta E = 0$. Solving the integral in Eq. (12) leads to

$$\Delta E = aA(\omega\mu_e - \omega^2\mu_s) \tag{13}$$

In Fig. 1(b), ΔE is plotted as a function of ω and several physical configurations of a cube at different values of ω are illustrated schematically. Differentiation of Eq. (13) with respect to ω shows that ΔE has a maximum when

$$\omega_{max} = \frac{\mu_e}{2\mu_s} = \frac{1}{2\rho\xi} = \frac{R^*}{2R\xi} \tag{14}$$

The nucleus size ω corresponding to the maximum of ΔE falls within the facet provided $1/2 < \rho\xi$; it will be seen that this condition is always fulfilled in our numerical calculations. The value of the maximum represents the barrier E^+ to layer addition and is given by

$$E^+ = \frac{aA\mu_e^2}{4\mu_s} = \frac{aA\sigma^2}{R^2\mu_s} = \frac{a\alpha\sigma R^*}{2\xi} \tag{15}$$

Here we have introduced the geometrical factor $\alpha = A/R^2$ which is proportional to the solid angle subtended by the facet at the crystal center. For a circular facet of radius r, Eq. (15) becomes $E^+ = a\pi\sigma R^*/2\xi$, whereas for a cube with L on a side, it becomes $E^+ = 2a\sigma R^*/\xi$. Both expressions can be easily verified by an independent calculation.

The lowest free energy path for layer removal proceeds by removal of an annular strip of atoms beginning at the facet edge and moving inwards, always leaving a partial layer of the same shape as the facet. The maximum again occurs at the value given by Eq. (14), but the free energy required is now given from Eq. (12) by $E^- = E^+ - \Delta E(\omega_{max})$. The result may be shown (see Appendix) to be

$$E^- = E^+\{1 + 4\rho\xi(\rho\xi - 1)\} \tag{16}$$

valid if $\rho\xi \ge 1/2$; for $\rho\xi \le 1/2$, E^- vanishes. With the use of Eq. (16), Eq. (11) may be written in the form

$$I = Ce^{-\beta/\xi}(1 - e^{-4\beta\rho(\rho\xi - 1)}) \tag{17}$$

where

$$\beta = \frac{E^+\xi}{kT} = \frac{a\alpha\sigma R^*}{2kT} \tag{18}$$

To get the growth rate due to nucleation, we assume that each nucleation event quickly results in the addition or subtraction of one atomic layer. Thus, we multiply I by a factor representing the volume of the new layer, Aa.

$$\dot{R}_{nuc} = aAI \tag{19}$$

Next, we need to estimate C in Eq. (17), which is given from nucleation theory by

$$C = Zn_m g \tag{20}$$

in which Z is the Zeldovich factor, n_m is the density of monomers on the facet, and g is the rate at which critical nuclei become supercritical. Since the nucleation rate is many orders of magnitude more sensitive to the barrier heights appearing in the exponentials than to the value of the prefactor C, the following very rough estimate of C suffices. We replace n_m by n_0, the number of atomic sites per unit area, and use $g = n_0 baf_0$, in which b is the perimeter of the critical nucleus and f_0 is the order of the jump frequency of an adatom or layer vacancy on the surface. We estimate b from the last member of Eq. (15) by regarding the energy as the product of the energy per unit length $a\sigma$ and a length $b \approx \alpha R^*/2\xi$ with $\alpha = 1$. Then with $Z = 10^{-2}$, the usual value, and $a = 10^{-10}$ m, we get $C \approx 10^{41} R^*/\xi$. Finally, with the above values, we obtain

$$\dot{R}_{nuc} = [10^{31}(R^*)^3\rho^2/\xi]e^{-\beta/\xi}\{e^{-E^+/kT} - e^{-E^-/kT}\} \tag{21}$$

(4) Solution of the Two Processes in Series

Equating and rearranging Eqs. (10) and (21) we obtain

$$\frac{\xi(1-\xi)}{\rho^3} = Be^{-\beta/\xi}(1 - e^{-4\beta\rho(\rho\xi - 1)}) \tag{22}$$

where $B = \alpha Za^2(R^*)^5 n^2/A_{diff}$. If we use the value $A_{diff} = 10^{-21}$ m^3/s, given after Eq. (10), Eq. (22) becomes

$$\frac{\xi(1-\xi)}{\rho^3} = 10^{52}(R^*)^5 e^{-\beta/\xi}(1 - e^{-4\beta\rho(\rho\xi - 1)}) \tag{23}$$

For a fixed R^*, Eq. (23) is to be solved for ξ as a function of ρ. Substitution back into Eq. (5) gives the growth rates represented by Eq. (6).

At this point, a few comments about Eq. (22) are appropriate. If $\rho = \xi = 1$, both sides vanish corresponding to equilibrium; note, the term representing the barrier for layer removal is essential for the RHS to vanish at equilibrium. Next, to get a rough estimate of the condition under which growth stops, note that under growth conditions, $\rho > 1$, $\xi < 1$, $\rho\xi > 1$. Therefore, the exponent $-4\beta\rho(\rho\xi - 1)$ on the right-hand side of Eq. (22) is negative and the exponential may typically be neglected, leaving $Be^{-\beta/\xi}$. This expression decreases rapidly as a function of R^* around the value of unity so that a rough estimate of the cutoff value of R^* above which growth effectively stops is given by solving

$$Be^{-\beta/\xi} = 1 \tag{24}$$

for R^* (note as R^* increases, typically B increases, β increases, and ξ decreases). Under dissolution conditions, on the other hand, the exponent is positive so that to match reasonable values on the left, we must have $\rho\xi$ barely below unity, which is the condition for diffusion-limited transfer. We see that the exponent $-4\beta\rho(\rho\xi - 1)$ (coming from the NEB for layer removal) acts something like a switch, changing sign at $\rho = 1$ and thereby distinguishing growth from dissolution behavior.

III. Computational Method

Let $n(R,t)\,dR$ be the number of particles of size between R and $R + dR$ at time t and let $v(R,R^*) = dR/dt = \dot{R}_{diff}$ be the velocity along the R axis of a particle as a function of its size, R, and R^*, or, equivalently, of ρ and R^*. The continuity equation that describes the evolution of the distribution, $n(R,t)$, is

$$\frac{\partial n}{\partial t} = \frac{-\partial(vn)}{\partial R} \tag{25}$$

where vn is the flux of particles along the R axis.

We assume that the total volume of particles is fixed. The value of R^* is chosen to achieve this. Thus, using Eq. (25) and integrating by parts,

$$\frac{\mathrm{d}}{\mathrm{d}t}\left(\int_0^\infty R^3 n(R,t)\,\mathrm{d}R\right) = -\int_0^\infty R^3\left[\frac{\partial(vn)}{\partial R}\right]\mathrm{d}R$$

$$= 3\int_0^\infty R^2[v(R,R^*)\,n(R,t)]\,\mathrm{d}R = 0 \quad (26)$$

Since v increases from negative values for $R < R^*$ to positive values for $R > R^*$, it is clear that if most of the particle distribution is larger than R^*, the integral in Eq. (26) will be positive, while if most of the distribution is smaller than R^*, the integral will be negative. Therefore, an intermediate value of R^* will exist for which the integral vanishes. When that value of R^* is used in $v(R, R^*)$, Eq. (25) upon integration gives the distribution in the next instant of time. A new value of R^* must then be sought and the process repeated.

To accomplish this procedure, it was first necessary to discretize the distribution by particle size. In the simulations, all particles were taken to be cubic. It was assumed that for each layer nucleation event, a square layer would instantly cover the nucleating facet, thus adding the volume equivalent of one layer $(a(2R)^2)$ to the existing cubic particle. To maintain the cubic shape and create discrete size classes of particles, it was assumed that this new layer volume was uniformly spread over the entire particle. Therefore, R was incremented as follows:

$$R_1 \cong 0, \quad R_2 = a, \quad \ldots$$

$$R_{i+1} = \frac{1}{2}\left((2R_i)^3 + a(2R_i)^2\right)^{1/3}, \quad \ldots \quad (27)$$

Clearly, it is inaccurate for the smallest particles to be treated as bulk-like, but for the purpose of demonstrating our hypothesis, we use a continuum treatment down to the smallest sizes. The negligible R_1 size enabled us to track the number of dissolving particles and avoided the need to choose an arbitrary small size for which to cut off the continuity integral.

So, prior to each time integration step, the value of R^* was determined as follows. First, we rearrange Eq. (22) and rewrite it explicitly in terms of R_i and R^*:

$$\frac{A_{\mathrm{diff}}\xi(R_i)(1-\xi(R_i))}{R_i R^*} - \left(\frac{CaR_i^2R^*}{2}\right)e^{-KR^*/\xi(R_i)}$$

$$\times\left[1 - e^{-K(4R_i[(R_i/R^*)\xi(R_i)-1])}\right] = 0 \quad (28)$$

Here, $K = \beta/R^*$. A trial R^* is chosen (initially 1 Å and subsequently the value of R^* from the prior timestep) and inserted into the series of equations embodied by Eq. (28). Equation (28) was then solved for $\xi(R_i)$ from which $v(R_i, R^*)$ can be calculated using Eq. (10). Changing the volume conservation criterion resulting from the continuity equation from an integral to a sum, we have

$$S = \sum_{i=1} 3R_i^2 n(R_i)\,v(R_i,R^*) = 0 \quad (29)$$

R^* is then iteratively adjusted by the false position method[6] to assure that the criterion that S equals zero is met.

After solving for R^* and the corresponding values of $\xi(R_i)$, one time integration step is taken. We used a semi-implicit extrapolation method for integration.[6] To discretize the continuity equation (Eq. (25)), modified upwind differencing was applied in the spirit of Muhr *et al.*[7] Our method differs somewhat from theirs because they used a constant spacing between particle size classes, while our spatial unit, $R_{i+1} - R_i$, increases with R, as can be seen in Eq. (27) above. Abbreviating $v(R_i, R^*)$ as v_i, v_L and v_R were defined as

$$v_L = \frac{v_{i-1} + v_i}{2} \quad (30a)$$

$$v_R = \frac{v_i + v_{i+1}}{2} \quad (30b)$$

The time derivatives were defined as follows:

For v_L and $v_R < 0$

$$\frac{\partial n_i}{\partial t} = -n_i\left(\frac{v_{i+1} - v_i}{R_{i+1} - R_i}\right) - v_i\left(\frac{n_{i+1} - n_i}{R_{i+1} - R_i}\right) \quad (31)$$

For v_L and $v_R > 0$

$$\frac{\partial n_i}{\partial t} = -n_i\left(\frac{v_i - v_{i-1}}{R_i - R_{i-1}}\right) - v_i\left(\frac{n_i - n_{i-1}}{R_i - R_{i-1}}\right) \quad (32)$$

For $v_L \leq 0$ and $v_R \geq 0$

$$\frac{\partial n_i}{\partial t} = -n_i\left(\frac{v_{i+1} - v_{i-1}}{R_{i+1} - R_{i-1}}\right) - v_i\left(\frac{n_{i+1} - n_{i-1}}{R_{i+1} - R_{i-1}}\right) \quad (33)$$

It can be seen that for dissolving particles (Eq. (31)), the rates are dependent only on the dissolving size class, i, and one size class greater. Smaller size classes do not impact the time evolution of the number of dissolving particles. Likewise, larger size classes do not impact the time evolution of the number of growing particles (Eq. (32)). This is accomplished by the upwind differencing. However, the time evolution of the number of particles of size R^* (Eq. (33)) is affected by the number densities of both smaller and larger particles.

To simulate the simultaneous evolution of defect-free particles and particles having surface defects, we assumed that there was no NEB for the surfaces of defect-bearing crystals. The NEB was rendered negligible for the defective crystals by assuming an unrealistically low surface energy for the barrier calculation. Thus, in Eq. (28), defect-free and defective particles share the same surface energy in A_{diff}, but the surface energy incorporated in K differs between the two populations. All particles were considered otherwise equivalent and all rate equations were solved simultaneously, including both populations in the continuity equation together.

IV. Results

We first consider the classical case of a set of particles coarsening without a NEB. In our model, we can "turn off" the NEB by choosing an unrealistically low surface energy. For example, if the surface energy is set to 0.001 J/m^2, the NEB becomes negligible and we can, therefore, approximate diffusion-limited particle growth rather than NEB-limited particle growth. The results of two such simulations, starting with different initial distributions of particles, are shown in Fig. 2. After the characteristics of the initial distribution have vanished, R^* increases with the cube root of time, as predicted by LSW theory[1,2] (see Fig. 3). In these simulations, large number densities of smaller particles steadily gave way to smaller number densities of larger particles. The initial distribution of the particles had no impact on the results, as illustrated in Fig. 2, nor did it impact subsequent results to be discussed.

To simulate NEB-limited particle growth, we assumed a surface energy of 0.1 J/m^2 and started with the same initial particle distribution as in Fig. 2(a). As can be seen in Fig. 4, all of the particles smaller than R^* eventually dissolved, while the largest particles could not grow past approximately 31 nm. Furthermore, as reflected in Fig. 5, R^* increases until it reaches a constant value and, having no more dissolving particle mass to draw from, the

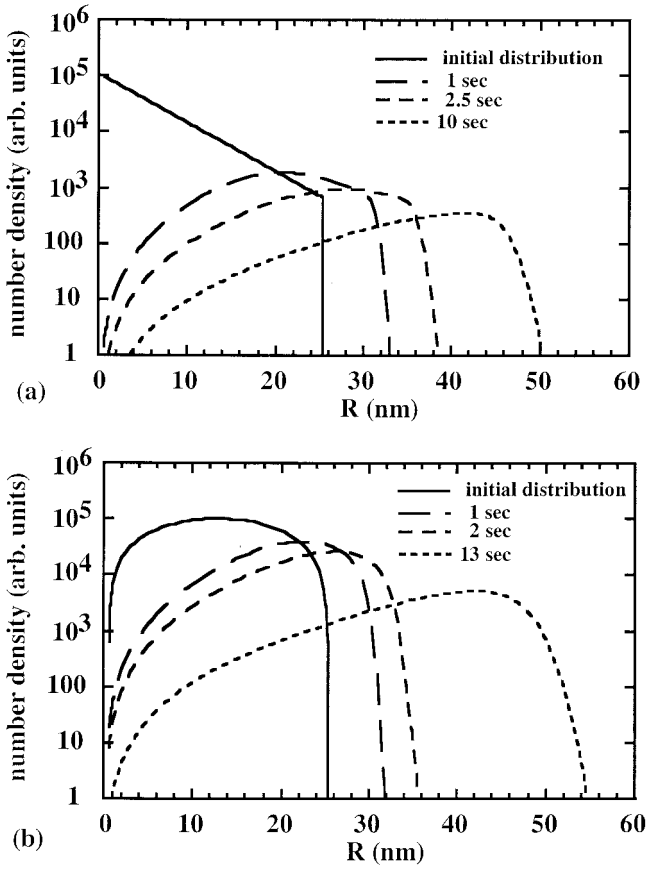

Fig. 2. Time evolution of two different initial distributions of particles. In (a) the initial distribution is exponential, and in (b) it is sinusoidal. In these simulations, the surface energy was 0.001 J/m^2, and the growth was diffusion limited.

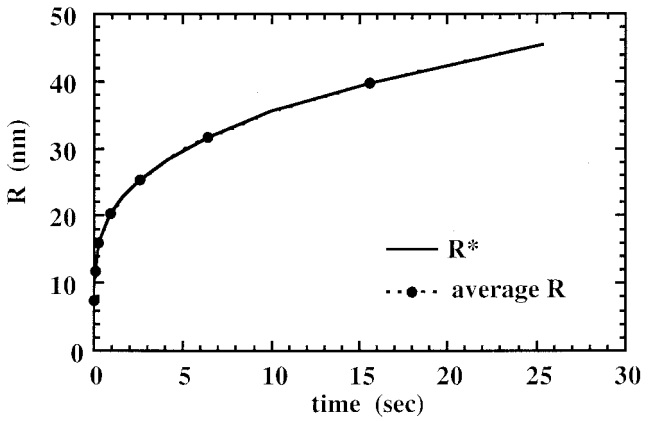

Fig. 3. Time evolution of the average particle radius and R^*, for the initial distribution in Fig. 2(a). The curves for the average radius and R^* overlap on the scale of this plot.

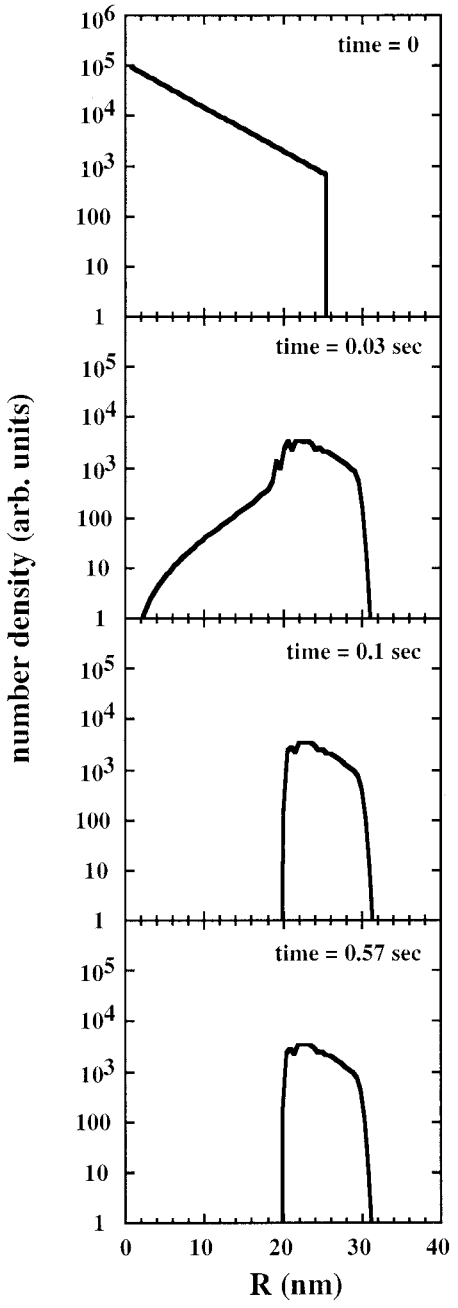

Fig. 4. Time evolution of a particle distribution when the surface energy is taken to be 0.1 J/m^2. In this case, the growth is NEB limited.

entire population distribution becomes static. The NEB effectively stops the coarsening of the particles.

Since a collection of many perfect, defect-free crystals is not likely to occur in nature, we simulated the effect of having a small population of defect-bearing particles among the majority of defect-free particles. It was assumed that the defect-bearing particles could grow without a NEB; this assumption was incorporated into the model as described above by using different surface energies for the two different populations in the nucleation rate equation. The NEB for defective particles was calculated using a surface energy of 0.001 J/m^2, while a value of 0.1 J/m^2 was used for the ideal particles. Note that a constant value of the surface energy (0.1 J/m^2) was used to determine the driving force for diffusion so that both defect-bearing and ideal particles of the same size were subjected to the same driving force. The results are shown in Fig. 6. Up to a point, the evolution of each population followed the trends of each population in isolation. The defect-free population could not grow bigger than approximately 31 nm and the defective population continued to grow unhindered. However, because the two populations share mass, defect-free particles began to dissolve (shown at 0.11 s), allowing the number densities of the larger defective particles to remain relatively constant. When this source of mass was not present for the defective particles, as in Fig. 2, the number densities of the larger particles decreased with time. The corresponding particle radius evolution is shown in Fig. 7. The average radius increases as particles smaller than R^* dissolve, but then begins to decrease again as the

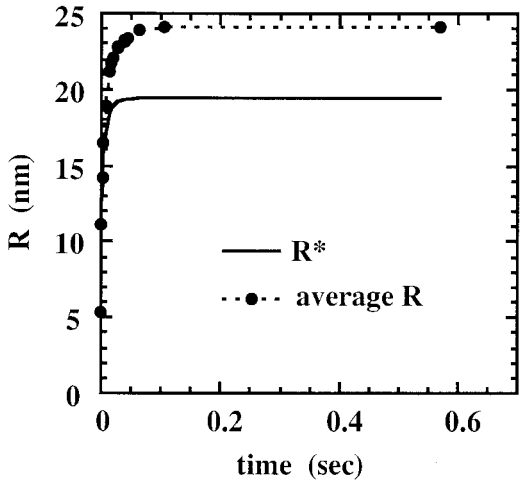

Fig. 5. Time evolution of the average particle radius and R^*, for the evolution of the distribution in Fig. 4. Growth stops when R^* reaches a critical size.

defect-free particles are sacrificed for the growth of the defective particles.

These results support the hypothesis that step-producing defects are responsible for the development of bimodal grain size distributions during the coarsening of faceted particles. If this is true, then the number density of the abnormal grains should remain constant until they consume the smaller grains. After this happens, none of the remaining "abnormal" grains should have an advantage over any of the others and continued coarsening should be normal. This is one feature of the simulation results that should be subject to experimental validation.

V. Discussion

Previous researchers have also considered how the coarsening of faceted particles, which might be influenced by an NEB, differs from the classical coarsening of particles with rough surfaces. We begin our discussion by pointing out one characteristic of the current model that distinguishes it from the earlier work. First, our model treats the dissolution (or evaporation) process differently than the previous work. According to Hirth and Pound,[8] "nucleation is not required to supply evaporation steps because they can arise at the edges of a clean, singular surface." This idea has been adopted by others in their work on coarsening.[9–11] However, we have previously argued that this statement cannot be correct in all circumstances.[4,5] For example, at equilibrium, the addition of a layer by the nucleation of a step loop that spreads to the edges of the facet, and the removal of a layer by the shrinking of a step loop from the edges of the facet to the center create identical instantaneous configurations. These identical configurations must have the same energy. Therefore, for either process to occur, they must pass through a relatively higher energy state that represents the NEB. This argument has been extended to nonequilibrium shapes and we have found that significant barriers persist far from equilibrium.[5] In the coarsening model described here, the NEB for the addition and removal of a layer are identical for a particle with size R^*. For particles smaller than R^*, the barrier for layer removal diminishes with R and disappears altogether for a particle for which $\rho\xi \leq 1/2$ (approximately $R \leq (1/2)R^*$).

The role of two-dimensional nucleation and defect-assisted growth in the abnormal coarsening of faceted particles has been discussed qualitatively in a number of papers during the last 5 years.[11–14] Park *et al.*[11] identified two factors as potentially leading to the abnormal coarsening of WC particles in liquid Co: defect-assisted growth and growth by two-dimensional nucleation. They assumed that two-dimensional nucleation could occur on the very largest particles in the distribution, as long as the mean field

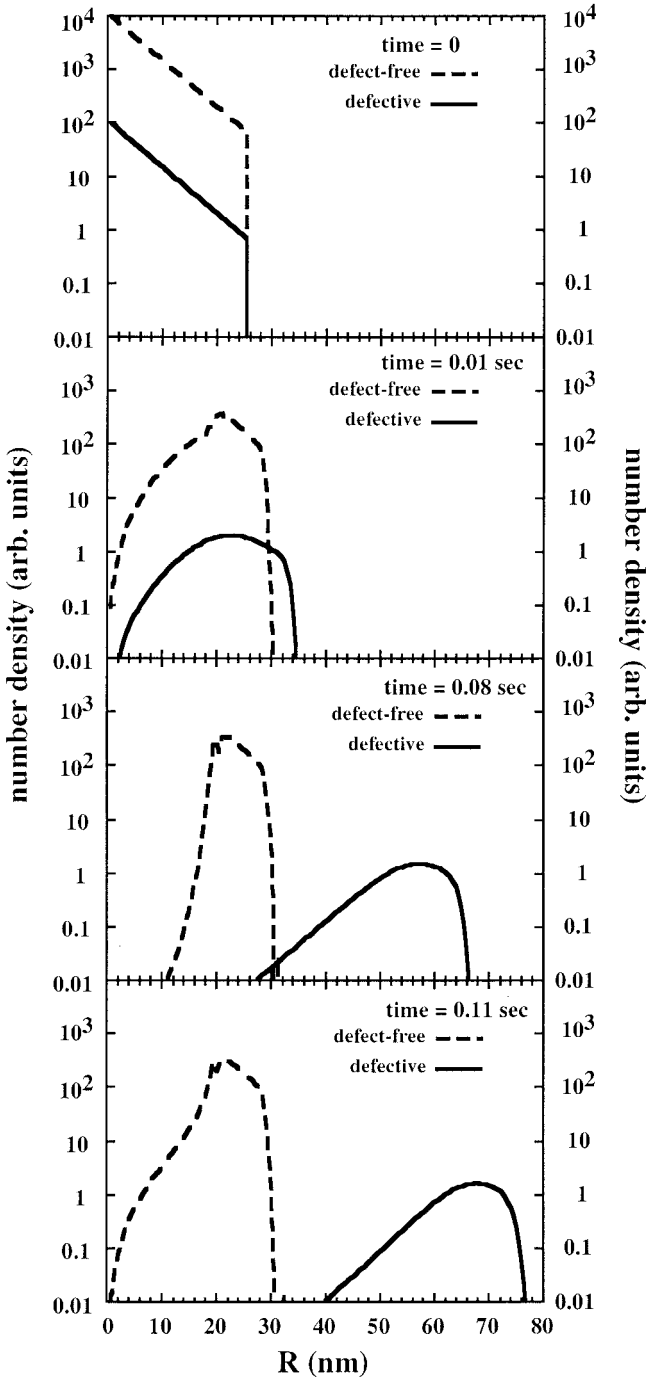

Fig. 6. Simultaneous evolution of the defect-free and defective particle populations.

chemical potential, as determined by R^*, remained large enough. They hypothesized that the extraordinarily high growth rate of the largest particles that are able to grow by two-dimensional nucleation, compared to those that cannot, leads to the bimodal grain size distribution characteristic of abnormal growth. They further suggest that when R^* rises above a critical value, and the chemical potential gradient is too small to drive two-dimensional nucleation on any particle, the bimodal distribution can be sustained by defect-assisted growth. While our calculations support the idea that the bimodal distribution is sustained by defect-assisted growth, we have not found evidence that abnormal growth in micrometer-sized particles can be caused by two-dimensional nucleation. Our results suggest that the critical R^* is in the range of a few nanometers to tens of nanometers (depending on the choice of physical parameters) and that abnormal growth in systems where

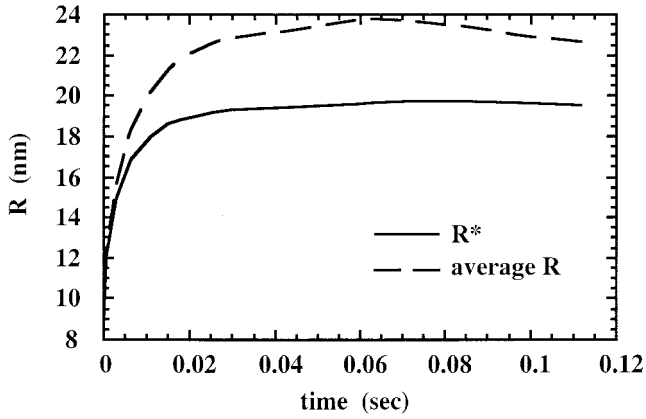

Fig. 7. Time evolution of the average particle radius and R^*, for the evolution of the distribution in Fig. 6.

R^* is in the vicinity of 1 μm (typical of the past experiments) must be entirely defect-assisted. In other words, abnormal growth is both initiated and sustained by defect-assisted growth.

Our conclusion that bimodal size distributions are created and sustained by defect-assisted growth is supported by previously reported results from experiments that probed the influence of particle shape and defect content on coarsening in a liquid medium.[11–16] Crystals bound by curved surfaces apparently coarsen in a classical manner while those bounded by facets sometimes exhibit abnormal coarsening.[12–14] However, studies of the influence of particle shape usually involve changes in the chemistry and or temperature that also potentially influence the kinetics. Defect-assisted growth has also been invoked as an explanation for abnormal growth.[11,14,15] The most well-documented examples concern the effects of twin plane reentrant edges in barium titanate[15] and dislocations in strontium titanate.[16] Our results support the explanation that faceted crystals larger than a few tens of nanometers must coarsen by a defect-assisted mechanism.

One of the assumptions in our model is that the crystals are fully faceted. We now ask how the model must be modified if we suppose that the ECS of the particle is only partially faceted. The new point is that the continuous part of the particle surface can exchange material with the medium without any NEB, thereby allowing the particle to change shape without any energy cost. The resulting shape evolution is essentially that described by classical crystal growth theory in which slow growing faces dominate in growth but shrink and disappear in dissolution. For example, a dissolving particle may lose all its facets without having to surmount any NEBs and then continue to shrink by diffusion alone.

A full treatment of the coarsening of partially faceted particles would require characterizing particles not only by size, but also by shape and then describing the evolution of all these size and shape parameters. Our focus in this paper, however, is on the cessation of coarsening as the particle size increases. As stated above, our numerical work, based on fully faceted particles, shows that this cessation does occur. The question is whether this basic conclusion is weakened in a system with partially faceted particles. We argue that in fact it is strengthened. That is because shape changes cause facets to predominate on growing particles, as discussed above, so that additional growth of these particles requires surmounting NEBs for layer addition.

Finally, our results allow us to speculate on the mechanistic underpinnings of the solid-state crystal conversion (SSCC)[17,18] and templated grain growth (TGG)[19,20] processes that are used to produce single-crystal or highly textured ceramic materials. In both cases, the relevant interesting observation is that when relatively large seed crystals are added to a fine polycrystalline matrix, the seeds or "templates" grow much more rapidly than the crystals in the matrix. According to results reported by Rehrig *et al.*,[20] barium titanate seeds can grow at rates as high as 790 μm/h, while the matrix grains grow at rates ≤9 μm/h, depending on the temperature. Since both of these processes frequently involve faceted crystals and growth occurs in the presence of an intergranular liquid phase, it is interesting to consider the experimental observations[17–20] in terms of the predictions from the coarsening model described here. While the mean field chemical potential approximation used in our simulations is not expected to be valid in the TGG and SSCC experiments, observations reported by Cho and Ardell[21] show that the rate of coarsening of cuboidal precipitates is not greatly influenced by the volume fraction of the particles. Therefore, it is not unreasonable to expect qualitative agreement between our simulations and the experiments.

Considering the fact that the initial matrix grain size is typically reported to be on the order of 2 μm, the capillary driving force from the matrix is not sufficient to drive two-dimensional nucleation on a flat facet of the seed. Instead, we suggest that a defect mechanism is responsible for observed higher growth rates of the seeds. The probability that any grain will have threading dislocations that impinge on the surface and create step sources will scale with the grain size. In a seed with lateral dimension of 1 mm or more, the presence of appropriate dislocations is virtually guaranteed. On the other hand, most of the 2 μm grains are unlikely to have such a dislocation. Although a few of the small grains will have threading dislocations, most will not and, as a result, the average grain size of the matrix will increase more slowly than the large seed. When the few fast growing matrix grains have enlarged to impingement and dominate the matrix population, the seed will no longer have a significant advantage and rapid growth should cease.

While the model presented here is not currently suitable to simulate solid precipitates in a solid matrix, anisotropic crystals, or grain growth in single-phase systems, it is interesting to consider the possibility that nucleation-controlled growth influences these processes. For example, it has already been suggested that dislocations at the solid–solid interface are responsible for the morphological instability of faceted NbC precipitates in Ni–Cr alloys.[22] Anisotropic coarsening, observed in Si_3N_4,[23] might result when the motion of some facets on a crystal is limited by an NEB while the motion of others is not. Finally, the increasing probability that larger crystals contain step-producing defects that minimize the influence of the NEB might explain the observed grain size dependence of the grain boundary mobility in alumina.[24]

VI. Summary

We have developed a numerical procedure to model the coarsening of faceted particles under the assumption that transport to and nucleation on the facet must occur in series. For crystals containing step-producing defects where there is no nucleation energy barrier, the growth is diffusion limited. For perfect crystals, the NEB limits growth when R^* is larger than a few tens of nanometers. When ideal and defect-containing crystals coarsen simultaneously, the defective crystals can grow at a rate limited by diffusion and a bimodal grain size is established. The results suggest that when faceted ceramic materials coarsen in a liquid medium, the grains that grow abnormally (much faster than others) are those that contain step-producing defects that impinge on the flat facets. The results suggest that if the growth of abnormal grains is completely defect controlled, as assumed here, then the number density of abnormal crystals should be constant during growth. Furthermore, the bimodal grain size distribution characteristic of abnormal coarsening should evolve to a normal distribution when all of the perfect crystals have been consumed.

Appendix

Again assume the nucleus has the same shape as the facet, but is smaller by the linear scale factor, ω ($0 \leq \omega \leq 1$), representing the size of the nucleus relative to the size of the facet. The energy

required to transfer a strip of material from the complete facet to a reservoir of chemical potential, μ_s, leaving a nucleus of size $\omega^2 Aa$ is

$$\Delta E = (\omega - 1)a\oint\sigma_p \, dl + (1 - \omega^2)Aa\mu_s \quad \text{(A-1)}$$

where the symbols have the same meaning as in Eq. (12). Differentiation shows the maximum to lie at $\omega_{max} = J/2A\mu_s$, where we have used J to stand for the integral. The corresponding maximum of ΔE, which is the barrier for layer removal, is

$$E^- = aJ^2/4A\mu_s - aJ + Aa\mu_s \quad \text{(A-2)}$$

But we know that removal of a complete layer ($\omega = 0$) from a facet at equilibrium ($\mu_s = \mu_e$) produces no energy change ($\Delta E = 0$). Use of these values in Eq. (A-1) gives $J = A\mu_e$. Finally, use of this relation and $\rho\xi = \mu_s/\mu_e$ in Eq. (A-2) gives

$$E^- = E^+[1 + 4\rho\xi(\rho\xi - 1)] \quad \text{(A-3)}$$

valid for $1/2 \leq \rho\xi$; if $\rho\xi \leq 1/2$, the barrier vanishes.

List of Symbols

L	Edge length of the crystal
R	Half edge length of the crystal ($L/2$)
R'	Radius of spherical shell superimposed on each particle
σ	Surface energy of the crystal
μ_∞	Mean field chemical potential
μ_e	Equilibrium chemical potential for each crystal ($2\sigma/R$)
μ_s	Chemical potential on the surface of the spherical shell
R^*	Size of particle in equilibrium with the medium ($2\sigma/\mu_\infty$)
ρ	R/R^*
ξ	μ_s/μ_∞
$\dot{R}_{diff}$	Growth rate of the particle due to diffusion
$\dot{R}_{nucl}$	Growth rate of the particle due to nucleation
$\dot{R}$	Growth rate of the particle
f_d	$(\mu_\infty - \mu_s)/(\mu_\infty - \mu_e)$
f_n	$(\mu_s - \mu_e)/(\mu_\infty - \mu_e)$
c	Concentration of solute in the medium
D_m	Diffusion coefficient of the solute in the medium
Ω	Atomic volume
k	Boltzmann's constant
T	Absolute temperature
A_{diff}	$2\sigma cD_m\Omega/kT$
I	Nucleation rate per unit area per unit time
E^+	Nucleation barrier for the addition of a layer
E^-	Nucleation barrier for the removal of a layer
ΔE	Free energy to form a nucleus of the same shape as the facet
ω	Linear scale factor proportional to the nucleus size
ω_{max}	Value of ω for the maximum of ΔE
σ_p	Orientation-dependent perimeter energy of the nucleus
a	Height of the nucleus
A	Facet area
α	A/R^2
β	$a\alpha\sigma R^*/2kT$
Z	Zeldovich factor
n_m	Density of monomers on the facet
g	Rate at which critical nuclei become supercritical
C	Znv
n_0	Number of atomic sites per unit area
b	Perimeter of the critical nucleus
f_0	Jump frequency of an adatom or layer vacancy on the surface
B	$\alpha Za^2(R^*)^5n^2/A_{diff}$
$n(R, t)$	Number of particles of size R at time t
v	Time rate of change of the particle radius, dR/dt
K	β/R^*

References

[1]I. M. Lifshitz and V. V. Slyozov, "The Kinetics of Precipitation from Supersaturated Solid Solutions," *J. Phys. Chem. Solids*, **19** [1/2] 35–50 (1961).

[2]C. Wagner, "Theory of Precipitate Aging via Dissolution/Reprecipitation; Ostwald Ripening," *Z. Electrochem.*, **65** [7/8] 581–91 (1961).

[3]W. K. Burton, N. Cabrera, and F. C. Frank, "The Growth of Crystals and the Equilibrium Structure of Their Surfaces," *Philos. Trans. R. Soc. London, Ser. A*, **243**, 300–58 (1951).

[4]W. W. Mullins and G. S. Rohrer, "Nucleation Barrier for Volume Conserving Shape Changes of Faceted Crystals," *J. Am. Ceram. Soc.*, **83** [1] 214–16 (2000).

[5]G. S. Rohrer, C. L. Rohrer, and W. W. Mullins, "Nucleation Energy Barriers for Volume Conserving Shape Changes of Crystals with Nonequilibrium Morphologies," *J. Am. Ceram. Soc.*, **84** [9] 2099–104 (2001).

[6]W. H. Press, S. A. Teukolsky, W. T. Vetterling, and B. P. Flannery, *Numerical Recipes in Fortran 77*; pp. 349 and 737. Cambridge University Press, Cambridge, U.K., 1996.

[7]H. Muhr, R. David, J. Villermaux, and P. H. Jezequel, "Crystallization and Precipitation Engineering—VI. Solving Population Balance in the Case of the Precipitation of Silver Bromide Crystals with High Primary Nucleation Rates by Using the First Order Upwind Differentiation," *Chem. Eng. Sci.*, **51** [2] 309–19 (1996).

[8]J. P. Hirth and G. M. Pound, Progress in Materials Science, Vol. 11, *Condensation and Evaporation, Nucleation and Growth Kinetics*; pp. 77–184. Pergamon Press, Oxford, U.K., 1963.

[9]P. Wynblatt and N. A. Gjostein, "Particle Growth in Model Supported Catalysts—I, Theory," *Acta Metall.*, **24** [12] 1165–74 (1976).

[10]P. Wynblatt, "Particle Growth in Model Supported Catalysts—II, Comparison of Experiment with Theory," *Acta Metall.*, **24** [12] 1175–82 (1976).

[11]Y. J. Park, N. M. Hwang, and D. Y. Yoon, "Abnormal Growth of Faceted (WC) Grains in a (Co) Liquid Matrix," *Metall. Mater. Trans. A*, **27** [9] 2809–19 (1996).

[12]S.-K. Kwon, S.-H. Hong, D.-Y. Kim, and N.-M. Hwang, "Coarsening Behavior of Tricalcium Silicate (C_3S) and Dicalcium Silicate (C_2S) Grains Dispersed in Clinker Melt," *J. Am. Ceram. Soc.*, **83** [5] 1247–52 (2000).

[13]K.-S. Oh, J.-Y. Jun, D.-Y. Kim, and N.-M. Hwang, "Shape Dependence of the Coarsening Behavior of Niobium Carbide Grains Dispersed in a Liquid Iron Matrix," *J. Am. Ceram. Soc.*, **83** [12] 3117–20 (2000).

[14]B.-K. Lee, S.-Y. Chung, and S.-J. L. Kang, "Grain Boundary Faceting and Abnormal Grain Growth in $BaTiO_3$," *Acta Mater.*, **48** [7] 1575–80 (2000).

[15]M.-K. Kang, Y.-S. Yoo, D.-Y. Kim, and N.-M. Hwang, "Growth of $BaTiO_3$ Seed Grains by the Twin-Plane Reentrant Edge Mechanism," *J. Am. Ceram. Soc.*, **83** [2] 385–90 (2000).

[16]S.-Y. Chung and S.-J. L. Kang, "Effect of Dislocations on Grain Growth in $SrTiO_3$," *J. Am. Ceram. Soc.*, **83** [11] 2828–32 (2000).

[17]T. Li, A. M. Scotch, H. M. Chan, M. P. Harmer, S. Park, T. R. Shrout, and J. R. Michael, "Single Crystals of $Pb(Mg_{1/3}Nb_{2/3})O_3$–35 mol% $PbTiO_3$ from Polycrystalline Precursors," *J. Am. Ceram. Soc.*, **81** [1] 244–48 (1998).

[18]A. Khan, F. A. Meschke, T. Li, A. M. Scotch, H. M. Chan, and M. P. Harmer, "Growth of $Pb(Mg_{1/3}Nb_{2/3})O_3$–35 mol% $PbTiO_3$ Single Crystals from (111) Substrates by Seeded Polycrystalline Conversion," *J. Am. Ceram. Soc.*, **82** [11] 2958–62 (1999).

[19]M. M. Seabaugh, I. H. Kerscht, and G. L. Messing, "Texture Development by Templated Grain Growth in Liquid-Phase Sintered α-Alumina," *J. Am. Ceram. Soc.*, **80** [5] 1181–88 (1997).

[20]P. W. Rehrig, G. L. Messing, and S. Trolier-McKinistry, "Templated Grain Growth of Barium Titanate Single Crystals," *J. Am. Ceram. Soc.*, **83** [11] 2654–60 (2000).

[21]J.-H. Cho and A. J. Ardell, "Coarsening of Ni_3Sn Precipitates in Binary Ni–Si Alloys at Intermediate to Large Volume Fractions," *Acta Mater.*, **45** [4] 1393–400 (1997).

[22]J. Billingham and S. P. Cooper, "The Effect of Thermal Cycling on the Microstructural Stability of Unidirectionally Solidified Eutectic Composite," *Met. Sci.*, **15** [7] 311–16 (1981).

[23]M. Kitayama, K. Hirao, M. Toriyama, and S. Kansaki, "Experimental Evidence for the Anisotropic Ostwald Ripening of β-Silicon Nitride," *J. Am. Ceram. Soc.*, **82** [10] 2931–33 (1999).

[24]J. Rödel and A. M. Glaeser, "Anisotropy of Grain Growth in Alumina," *J. Am. Ceram. Soc.*, **73** [11] 3292–301 (1990). □